Surface Nanofeature Effects on Titanium-Adherent Human Mesenchymal Stem Cells

Sara Valencia, BS[1]/Christina Gretzer, PhD[2]/Lyndon F. Cooper, DDS, PhD[3]

Purpose*: Hydrofluoric acid treatment of moderately rough commercially pure titanium produced by titanium oxide (TiO$_2$) grit blasting (OsseoSpeed) results in a surface with nanofeatures. The aim of this project was to better understand the effect of surface nanotopography on adherent osteoblastic differentiation.* ***Materials and Methods****: Human mesenchymal stem cells were grown on TiO$_2$ grit−blasted and hydrofluoric acid−treated/TiO$_2$ grit−blasted titanium coins for 1 to 28 days. The nature of the surfaces was evaluated using scanning electron microscopy, optical interferometry, and x-ray photoelectron spectrometry. Osteoblastic differentiation was measured using real-time polymerase chain reaction measurement of more than 80 mineralized tissue−associated, protein-encoding mRNAs.* ***Results****: Hydrofluoric acid−treated surfaces displayed nanofeatures of 100 nm in diameter and maintenance of micron-level topography. Adherent cell osteoblastic differentiation occurred on both surfaces but took place more rapidly and to a greater extent on hydrofluoric acid−treated surfaces. This was revealed by earlier, higher, and sustained levels of osteoinductive transcription factors (RUNX-2, SMADs), growth factors (insulin-like growth factor 2, bone morphogenetic proteins), and bone matrix proteins.* ***Conclusions****: The superimposition of nanofeatures on a moderately rough commercially pure titanium surface is associated with marked osteoinduction and osteogenesis of adherent mesenchymal stem cells. The role of nanotopography in directing adherent cell behavior should be fully investigated.* INT J ORAL MAXILLOFAC IMPLANTS 2009;24:38−46

Key words: *commercially pure titanium, gene expression, human mesenchymal stem cell, nanotopography, osteoinduction, real-time polymerase chain reaction*

Improvement in osseointegration can be measured by the increased bone-to-implant contact (BIC) achieved at discrete time points following implant placement in bone. Clinical results from the earliest clinical trials indicated that low implant survival rates were observed where implants were placed in the lowest quality of bone. A relationship was suggested between the extent of bone accrual at the implant surface and ultimate implant survival. Based on these

perceptions, improvement of BIC is regarded as a useful strategy to enhance the results of implant therapy.

Albrektsson and Wennerberg[1] recently characterized implant surfaces based on the magnitude of the surface topographic modification. A range of topographic modifications was suggested to support greater BIC. Surfaces with characteristic topographies with features of approximately 1.5 to 2.0 μm offer enhanced BIC. Several different clinical implant systems with surfaces in the moderately rough topographic category show high survival rates in 5-year clinical investigations. Human histologic comparisons of bone accrual on moderately rough- versus minimally rough-surfaced implants indicated that as much as four times greater BIC was present at implants placed in lower-density posterior maxillary and mandibular bone after 6 months.[2]

Recent clinical innovations such as the immediate placement of implants in extraction sockets or procedures that involve immediate loading of implants

[1]Research Assistant, Dental Research Center, University of North Carolina at Chapel Hill.
[2]Research Scientist, Research and Development, AstraTech, Mölndal, Sweden.
[3]Stallings Distinguished Professor, Department of Prosthodontics, University of North Carolina at Chapel Hill.

Correspondence to: Dr Lyndon F. Cooper, 330 Brauer Hall CB7450, University of North Carolina, Chapel Hill, NC 27599-7450. Fax: +919-966-3821. Email: Lyndon_Cooper@dentistry.unc.edu

place greater emphasis on interfacial bone formation. As an example, the formation of bone in the gap that exists between an implant and an extraction socket was shown to occur for gap distances of 1.5 to 2.0 mm when a moderately rough implant was used, in contrast to the limiting gap distance of 0.5 mm measured previously at minimally rough machined commercially pure titanium (cpTi) implants.[3]

More rapid bone accrual may be required for contemporary implant procedures. The rate of bone formation may be accelerated in attempts to maintain implant stability under challenging clinical conditions. A wide array of concepts, including biologic activation of the titanium surface with cell-adhesive molecules or bone morphogenetic proteins, has been proposed.[4,5] Alternatively, further modification of the implant surface topography at the nanoscale has particular merit based on initial observations and simplicity.[6]

Zinger et al[7] introduced the concept of scale-resolved topography and described osteoblast-like cell behavior in terms of the topography magnitude. The study included large hemispheric pits of 10 to 100 µm in diameter onto which micron-dimension topography was superimposed by acid etching or anodization. The results suggest that osteoblastic cells interpret surface topography in select ranges of magnitude. True nanometer-scale topography was not investigated.

Nanotopography has been defined as surface topography with one feature with a magnitude of 100 nm or less.[8] Early investigations involving osteoblast responses to nanotopographic features were performed using anatase or rutile titanium that displayed different surface crystalline structure. Such nanoscale surfaces supported greater osteoblastic cell differentiation.[9] Oliveira et al[10] used a combination of acid etching and peroxidation to create true nanoscale topography on machined cpTi surfaces and observed greater osteoblastic differentiation of cells cultured on the nanotopography-modified surfaces.

Other approaches to improving osseointegration include the alteration of surface chemistry. At least two approaches have been considered. One is the coating of titanium implants, for example, with hydroxyapatite. Initial methods using plasma spraying with rough coatings (5 to 25 µm dimensions) on implants were used with limited approval and success.[11] More recently, ultrathin layers and nanosized features have been added by ion-beam deposition, plasma spray, and liquid phase adsorption or precipitation methods.[12–14] Both ion-beam deposition and liquid phase adsorption of calcium phosphate–nanofeatured surfaces have been translated to the dental implant marketplace, with the reported

advantage of improved BIC.[15] Surface chemistry can be altered ionically as well. Changes in both surface calcium and surface magnesium were evaluated by Sul et al,[16,17] and a calcium-modified titanium endosseous dental implant is available clinically.[15]

A hydrofluoric acid (HF)–modified titanium dioxide grit–blasted surface was recently introduced as a clinical dental implant (Osseospeed, AstraTech, Mölndal, Sweden). Although this implant surface modification results in the retention of approximately 1.0 atomic percentage (at %) fluoride on the implant surface, there is also the resultant formation of approximately 100-nm-diameter nanofeatures along the moderately rough titanium surface. The developmental research included observations of increased physical interaction with bone,[16] greater BIC,[17,18] and greater osteogenesis by implant-adherent cells.[19,20] The molecular basis for this enhancement is not fully appreciated; however, nanofeatures superimposed by HF treatment are presently implicated in altering adherent cell behavior.

Another approach to modifying tissue interactions with alloplastic materials is through changes in surface energy. This basic physical approach changes the cell and fluid interactions with titanium implants.[21,22] The recent alteration of a grit-blasted/acid-etched titanium implant surface (SLActive, Straumann, Waldenburg, Switzerland) led to the measured enhancement of BIC that was attributed to changes in implant surface energy.[23]

The aim of the present experiment was to examine the effect of superimposing nanotopographic elements created by HF treatment onto a moderately rough cpTi surface on adherent human mesenchymal stem cells (MSCs). Gene expression related to osteoinduction was specifically evaluated using arrayed real-time polymerase chain reaction (PCR) assays.

MATERIALS AND METHODS

Cell Culture

Human MSCs were cultured in accordance with published protocols.[24] Growth media included Dulbecco's modified eagle medium, low glucose (Gibco, Gaithersburg, MD), supplemented with 10% fetal bovine serum and antibiotic/antimycotic (penicillin/ streptomycin/ amphotericin B, Sigma, St Louis, MO).

Osteogenic media included Dulbecco's modified eagle medium, low glucose (Gibco, #11885), supplemented with 10% fetal bovine serum, antibiotic/ antimycotic, and the osteogenic supplements 10 µmol/L dexamethasone, 10 µmol/L glycerophosphate (Sigma, #G9891), and 50 µg/mL ascorbic acid (Sigma,

#A4403). Passage 2 cells were plated at low density and grown until nearly confluent. Cells were subsequently passaged onto prepared titanium disks using 30,000 cells in 70 µL of growth media. The formed meniscus was left undisturbed to permit cell attachment over 4 hours, and subsequently additional growth media was applied. Following overnight incubation, cultures were carefully rinsed and osteogenic medium was placed in culture dishes. This represented the starting time point (T = 0). The osteogenic medium was replaced every third day. Disks with adherent cell and forming tissue layers were collected on days 7, 14, and 28.

Titanium Disk Preparation

One group of 6.25-mm-diameter titanium disks was prepared by blasting with titanium oxide (TiO_2) particles according to a proprietary manufacturing procedure (GB). The other group of 6.25-mm-diameter titanium disks was also blasted with TiO_2 particles in an identical manner and further subjected to HF treatment according to the OsseoSpeed manufacturing procedure (OS). All disks were cleaned and sterilized according to a clinical dental implant manufacturing procedure.

Titanium Disk Evaluation

Scanning electron microscopy (SEM) was used to describe the nature and dimension of surface nanofeatures. The three-dimensional topography of the specimens was characterized with optical interferometry (MicroXAM, PhaseShift, Tucson, AZ). The analysis was performed with a measurement area of 200×260 µm^2. Each specimen was analyzed in three areas, and three specimens of each surface type were analyzed. Errors of form were removed with a digital Gaussian filter.[25] The chemical nature of the surfaces was examined by x-ray photoelectron spectrometry (XPS). A Quantum 2000 ESCA SEM (Physical Electronics, Chanhassen, MN) with a monochromatic AlKα x-ray source was used to analyze OS and GB disks. A pass energy of 187.8 eV (highest sensitivity) was used to obtain spectra for C1s, O1s, Ti2p, F1s, N1s, and Si2p. MULTIPAK (Physical Electronics) was used to calculate the elemental composition in atomic percentages (at %). The sensitivity for fluorine is approximately 0.1 at %.

RNA Isolation

Upon sampling, wells containing disks were rinsed three times in ice-cold phosphate-buffered saline. The disks were immediately covered with 200 µL of RNA lysis buffer (Trizol, Invitrogen, Carlsbad, CA). Repeated pipetting was performed to remove the lysates from the disks. A second 200-µL aliquot of RNA lysis buffer was applied, and liquid was harvested from the disks by microcentrifugation at 6,500 rpm for 3 minutes at 4°C. RNA isolated by the Trizol method was precipitated with ethanol and stored until required for cDNA synthesis. After being resolved in RNAse-free diethylpyrocarbonate–treated water, the RNA was quantified by ultraviolet spectrophotometry. For all experiments, four independent cultures were established and evaluated on four disks at each time point.

Real-Time Polymerase Chain Reaction

Analysis of adherent cellular differentiation was performed at the level of mRNA expression. For this investigation, a broad analysis of osteoinductive and osteogenic protein gene expression was performed using the GE Superarray System (Superarray, Frederick, MD). It offers a real-time PCR format for simultaneous analysis of more than 80 genes and permits analysis using several different normalization strategies. Additional assessments of gene expression at 3 days were made using conventional real-time PCR reactions for Osterix, RUNX2, osteoprotegerin, and alkaline phosphatase. For day 3 studies, four cultures were evaluated at each time point.

Each real-time PCR reaction was programmed according to the manufacturer's protocol using cDNA synthesized from 3 µg of total RNA. The cDNA synthesis was performed using a standard superscript reverse transcription reaction. Thereafter, the cDNAs were diluted and 1-µL aliquots were distributed among the arrayed real-time PCR reactions.

RESULTS

The surfaces used in this study differed in terms of nanofeatures and displayed minor microscale topographic differences. Measurement of surface parameters showed the reduced microfeatures including, but not limited, to amplitude (S_a) of the HF-treated surfaces (Table 1). SEMs suggest the conservation of microfeatures on the two surfaces and further reveal the presence of discrete 50- to 200-nm nanofeatures on the blasted surface treated with HF. At high resolution, there is little nanotopographic character of the GB surface (Fig 1). XPS analysis identified fluoride at approximately 1.0 at % on the OS surface. This treatment also reduced the measured atomic percentage of carbon when compared to the TiO_2 grit–blasted surface (Table 2).

Cells were successfully grown and expanded on both the GB and OS surfaces. Cell layers were formed in multilayers and retraction from the disks was not observed. From the cultures established with 30,000

Table 1 Surface Roughness Values (Means and SDs) from Optical Interferometry Analyses

Surface modification	n	S_a (µm)	S_{ds} (µm^{-2})	S_{dr} (%)	S_{tr}
OS	9	1.46 (0.07)	0.140 (0.007)	55.33 (7.74)	0.65 (0.08)
GB	9	1.60 (0.15)	0.160 (0.009)	70.47 (12.42)	0.64 (0.05)

S_a (µm)= the arithmatic average height deviation from a mean plane; S_{ds} (µm^{-2}) = the density of summits; S_{dr} (%)= the developed surface ratio; S_{tr} = the uniformity of texture aspect.

Fig 1 Scanning electron micrographic images of the GB and OS surfaces used in this investigation. (*Left*) Low-power images reveal similar micron-level topography of the OS and GB surfaces, respectively. (*Right*) High-power images permit comparison of the nanolevel topography and reveal little nanostructure of the GB surface (*bottom right*) and approximately 100 nm accretions present on the OS surface (*top right*).
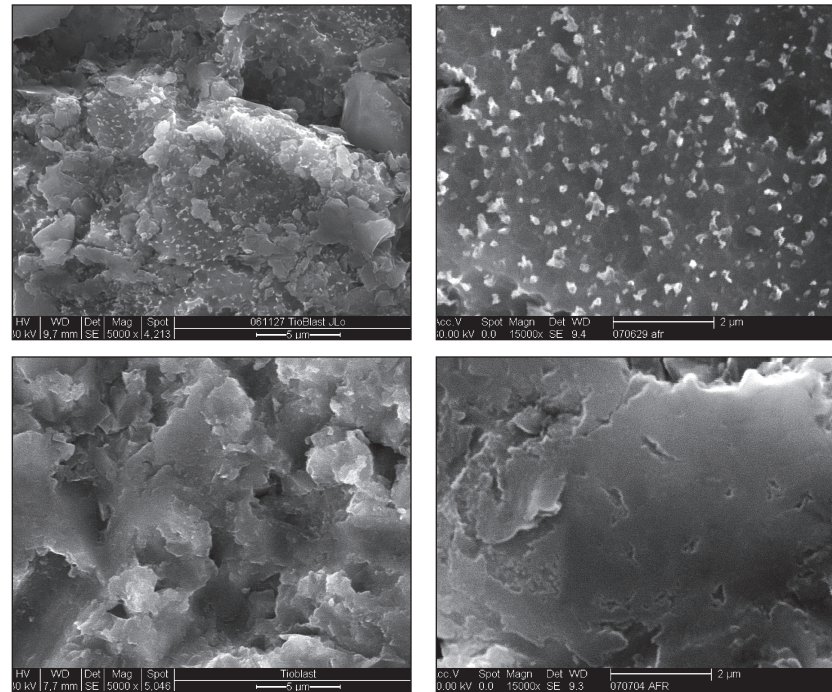
Table 2 Ion Composition Data (Means ± SDs) from XPS Analyses

Surface type	C1s	N1s	O1s	F1s	P2p	Ti2p
TiO	23.92 ± 4.0	0.27 ± 0.3	52.75 ± 2.14	-	-	22.73 ± 1.59
OS	21.7 ± 0.3	0.4 ± 0.3	53.6 ± 0.5	0.8 ± 0.2		23.6 ± 0.2

cells, there were sufficient numbers of cells present after 7, 14, and 28 days for isolation of total RNA (> 3 µg of total RNA) to perform the arrayed real-time PCR reactions.

The analysis of cellular phenotype at the level of mRNA abundance was performed and is presented by classification of groups of mRNAs according to the known or proposed function of the encoded protein. The categories are: growth factors, transcription factors, soluble ligand receptors, integrin receptors, bone matrix proteins, and transforming growth factor/bone morphogenetic protein (TGF/BMP) superfamily genes. One general observation was that early differences between the two surfaces (7 days) were often of lower magnitude than differences observed

at 14 and 28 days. The most prominent differences at 7 days were observed for several BMP-encoding mRNAs that were elevated on OS versus GB surfaces. A second overall observation was that the majority of bone-related or bone-specific mRNA levels were higher at 14 and 28 days in cells cultured on the OS surface. Exceptions were growth differentiation factor 10, insulin-like growth factor 1 (IGF1), epidermal growth factor (EGF), vascular endothelial growth factor B (VEGF B), and integrin β1.

Twelve receptor-encoding mRNA levels were monitored from cells grown on the two surfaces. At 7 days, 2- to 5-fold relative elevations were noted for cells grown on the OS surface. However, the epidermal growth factor receptor (EGFR) was elevated more
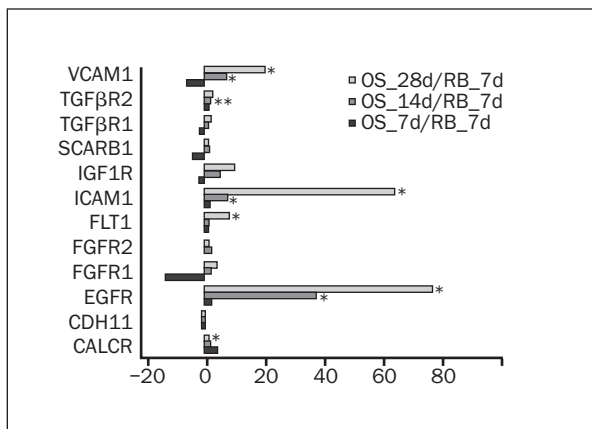
Fig 2 Relative expression of osteogenesis-related receptor-encoding cDNAs in cells adherent to OS versus GB surfaces at 7 days (*black bars*), 14 days (*gray bars*), and 28 days (*white bars*) in culture. Each gene of interest and its indicated magnitude is the fold elevation calculated as OS/GB real-time PCR quantification. Each data point is the average of 4 separate cDNA reactions programming individual PCR reactions. The receptor genes consist of vascular cell adhesion molecule I (VCAM1), transforming growth factor beta receptor II (TGFβ2), transforming growth factor beta receptor I (TGFβ1), scavenger receptor class B member 1 (SCARB1), insulinlike growth factor 1 receptor (IGF1R), intercellular adhesion molecule 1 (ICAM1) (CD54) human rhinovirus receptor, Fms-related tyrosine kinase 1 (vascular endothelial growth factor/vascular permeability factor receptor; FLT1), fibroblast growth factor receptor 2 (FGFR2), fibroblast growth factor receptor 1 (FGFR1), epidermal growth factor receptor (EGFR), cadherin 11 type 2 (CDH11), and calcitonin receptor (CALCR). *P < .05; **P < .001.

Fig 3 Relative expression of integrin receptor–encoding cDNAs in cells adherent to OS versus GB surfaces at 7 days (*black bars*), 14 days (*gray bars*), and 28 days (*white bars*) in culture. Each gene of interest and its indicated magnitude is the fold elevation calculated as OS/GB real-time PCR quantification. Each data point is the average of four separate cDNA reactions programming individual PCR reactions. The integrin receptor genes consist of integrin beta 1 (ITGβ1), integrin alpha 3 (ITGα3), integrin alpha 2 (ITGα2), and integrin alpha 1 (ITGα1). *P < .05.

than 30-fold at 14 days and more than 60-fold after 28 days. EGFR is a tyrosine kinase expressed in tissue skeletal development. It has been implanted in bone formation. EGFR-deficient mice (EGFR$^{-/-}$ mice) have impaired bone formation in part owing to delayed osteoblast recruitment.[26] Levels of both intercellular adhesion molecule 1 (ICAM1) and vascular cell adhesion molecule (VCAM1) were elevated at 14 and 28 days, whereas the osteoblast-specific cadherin levels differed minimally (Fig 2). ICAM1 and VCAM1 are recognized as important receptors affecting cell-cell interactions involved in bone metabolism, particularly as related to inflammatory signaling.

A subclass of receptors, the integrins, has been implicated in the relationship of cell phenotype to dental implant topography. Integrins are receptors for extracellular matrix proteins (eg, collagen, bone sialoprotein) that signal changes in osteoblast survival, cell-cycle progression, gene expression, and matrix mineralization. The levels of the β1, α1, α2, and α3 integrins were measured (Fig 3). Interestingly, β1 integrin levels were relatively suppressed at 14 days in cells grown on the OS titanium surface. In contrast, the α3 and α1 integrins were induced during this time period. This dynamic alteration in integrin expression most likely reflects the formation of a mul-
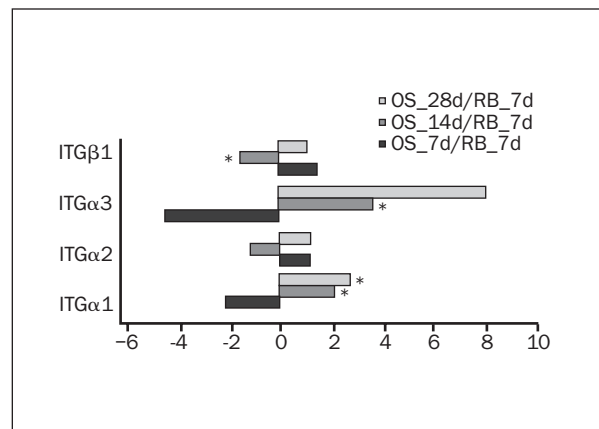
tilayered scaffold of cells within an extracellular matrix, where many of these interactions occur beyond the surface. The changes with time suggest that the surface-adherent nature of the cells and scaffolding affect the physiology of this complex tissue.

The relative levels of mRNAs encoding various growth factors were also compared (Fig 4). For most growth factors, higher levels were observed for RNAs of OS-adherent cells, with the key exception being VEGF B expression at 7, 14, and 28 days. Threefold or greater elevations in colony-stimulating factor 2, IGF1, IGF2, platelet-derived growth factor A, and VEGF were noted in 28-day samples from OS-adherent cells. Most notably, IGF2 levels were 2 times greater in OS-adherent cells at 14 days. IGF2 is well defined as a key factor in MSC osteogenesis and bone formation. It functions to promote proliferation and differentiation on osteoblasts.

Transcriptional control of osteoblastogenesis is clearly central to bone formation. The key factor controlling osteoblastic differentiation from undifferentiated stem cells is RUNX2. When RUNX2 levels were compared here, and higher steady-state levels of RUNX2 were noted for OS-adherent versus GB-adherent cells at 14 and 28 days (7-fold and 11-fold, respectively; Fig 5). Other transcription factors are critical to
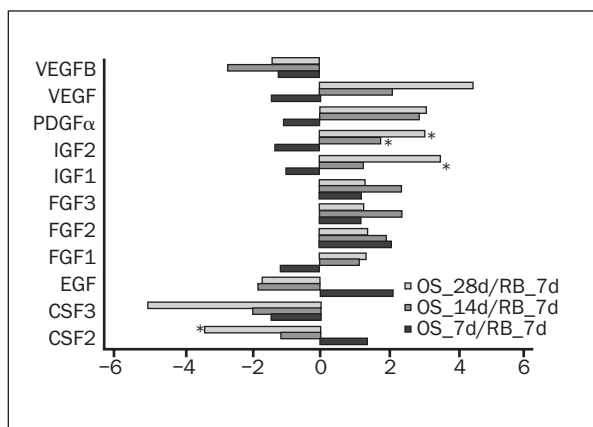
Fig 4 Relative expression of osteogenesis-related growth factor–encoding cDNAs in cells adherent to OS versus GB surfaces at 7 days (*black bars*), 14 days (*gray bars*), and 28 days (*white bars*) in culture. Each gene of interest and its indicated magnitude is the fold elevation calculated as OS/GB real-time PCR quantification. Each data point is the average of four separate cDNA reactions programming individual PCR reactions. The growth factor genes consist of vascular endothelial growth factor B (VEGFB), vascular endothelial growth factor (VEGF), platelet-derived growth factor alpha polypeptide (PDGFα), insulinlike growth factor 2 (IGF2), insulinlike growth factor 1 (IGF1), fibroblast growth factor 3 (FGF3), fibroblast growth factor 2 (basic; FGF2), fibroblast growth factor 1 (acidic; FGF1), epidermal growth factor (EGF), colony-stimulating factor 3 (CSF3), and colony-stimulating factor 2 (CSF2). *$P < .05$.
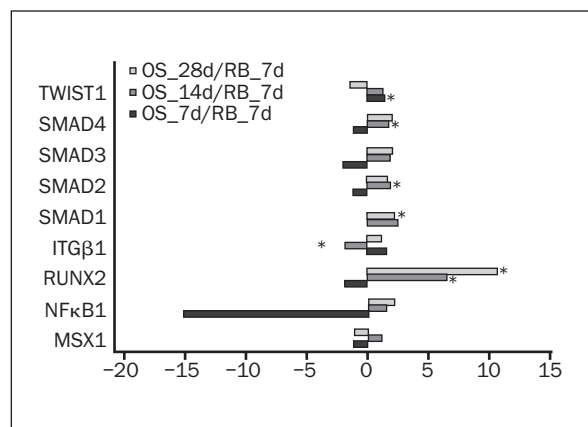

Fig 5 Relative expression of osteogenesis-related transcription factor–encoding cDNAs in cells adherent to Os versus GB surfaces at 7 days (*black bars*), 14 days (*gray bars*), and 28 days (*white bars*) in culture. Each gene of interest and its indicated magnitude is the fold elevation calculated as OS/GB real-time PCR quantification. Each data point is the average of four separate cDNA reactions programming individual PCR reactions. The transcription factor genes consist of twist homolog 1 (TWIST1), SMAD4, SMAD3, SMAD2, SMAD1, integrin beta 1 (ITGβ1), RUNX2, nuclear factor kappa B (NFκB), and Msh homeobox homolog 1 (MSX1). *$P < .05$.

osteogenesis, and BMP signaling of osteogenesis uses SMAD transcription factors to control osteogenesis. Notably, SMAD1 was present in greater abundance in OS-adherent than in GB-adherent cells at the 14- and 28-day time points, and SMAD4 abundance was parallel with SMAD1 and SMAD2 ($P > .05$, day 14).

The central regulatory factor controlling inflammatory signaling in all mammalian cells is nuclear factor kappa B (NFκB). NFκB activity may be detrimental to osteogenesis.[27] Here, the levels of NFκB1 mRNA were markedly lower (> 15-fold) at day 7 in OS-adherent cells (Fig 5).

The effect of superimposed nanotopography was also observed when comparing the levels of BMP superfamily–encoding mRNAs from GB- and OS-adherent cells (Fig 6). At day 7, approximately 5-fold greater expression was observed for BMP2, BMP4, and BMP6; BMP5 levels were nearly 15-fold greater. At 14 days, BMP2 and BMP6 mRNA levels were 30 and 15 times greater in OS-adherent cells. A continued disparity in BMP mRNA abundance was revealed after 28 days. At that time point, BMP2, BMP4, and BMP6 showed 35-, 15-, and 25-fold greater levels in cells cultured on the OS surface.

Measurement of bone matrix protein gene expression indicated that major differences occurred later in the culture period. By 14 days, all mRNA levels were significantly elevated. At 28 days, a 50-fold greater level of alkaline phosphatase expression was observed for the cultures formed on the OS surface (Fig 7). Alkaline phosphatase is a commonly employed marker of early osteoblastic differentiation. The continuously elevated levels suggest that the multicellular layer adherent to the nanoscale-modified surface has organized in a functionally significant manner that extends beyond the initial cell-surface interaction.

DISCUSSION

Nanofeatures can be imparted to moderately rough endosseous dental implant materials. Several different approaches include ion beam deposition, solution phase deposition, and surface modification based on oxidation or etching. The present investigation examined the effect of a nanofeature embellishment of TiO_2 grit–blasted titanium surfaces on cellular differentiation along the osteoblastic lineage. The 50- to 200-nm-diameter nanofeatures observed by SEM are consistent with the magnitude of other nanofeatures that have been shown to promote osteoblastic differentiation.[9]

This investigation used human MSCs to model osteoinduction and osteoblastic differentiation in cell
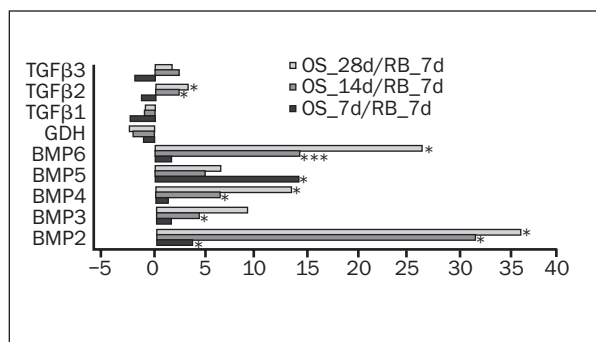
Fig 6 Relative expression of BMP superfamily-encoding cDNAs in cells adherent to OS versus GB surfaces at 7 days (*black bars*), 14 days (*gray bars*), and 28 days (*white bars*) in culture. Each gene of interest and its indicated magnitude is the fold elevation calculated as OS/GB real-time PCR quantification. Each data point is the average of four separate cDNA reactions programming individual PCR reactions. The BMP superfamily genes consist of transforming growth factor beta 3 (TGFβ3), transforming growth factor beta 2 (TGFβ2), transforming growth factor beta 1 (TGFβ1), growth differentiation factor 10 (GDF10), and BMP6, BMP5, BMP4, BMP3, and BMP2. *$P < .05$; ***$P < .0001$.

Fig 7 Relative expression of bone matrix extracellular protein–encoding cDNAs in cells adherent to OS versus GB surfaces at 7 days (*black bars*), 14 days (*gray bars*), and 28 days (*white bars*) in culture. Each gene of interest and its indicated magnitude is the fold elevation calculated as OS/GB real-time PCR quantification. Each data point is the average of four separate cDNA reactions programming individual PCR reactions. The bone matrix extracellular protein genes consist of osteocalcin (OCN), biglycan (BGN), alkaline phosphatase (ALPL), and alpha-2-HS-glycoprotein (αHSG). *$P < .05$.

cultures performed on two moderately rough titanium substrates, one of which possesses discrete nanofeatures. Specific osteoinductive culture conditions result in the reproducible osteoblastic differentiation of the MSC when cultured on tissue culture plastic dishes.[24] Cooper et al[19] used this model to explore the effect of titanium surface topography on adherent cell osteoblastic differentiation and showed that changes in bone matrix protein expression occur as a function of the titanium surface topography. Dalby et al[28] used a similar model—human bone marrow cells and osteogenic culture—to demonstrate the positive influence of nanotopography on adherent cell differentiation. They suggested that human mesenchymal populations are especially sensitive to nanocues requiring such extracellular cues for subsequent differentiation.

Other models have been used to examine nanotopography effects on adherent cell osteogenesis. Oliveira et al[10,29] examined the behavior of adherent rat calvaria osteoprogenitor cells on machined cpTi and nanotextured cpTi surfaces and observed greater osteogenesis in cell layers formed on the nanotextured surfaces. Both Oliveira and Dalby used immunofluorescence to examine bone-specific protein expression qualitatively. Isa et al[30] and Masaki et al[20] used human palatal mesenchymal cells to model osteoblastic differentiation on different titanium substrates. They observed higher levels of RUNX2 mRNA on a Ti grit–blasted and HF-treated surface (similar to OS studied here) and suggested that implant surface treatment may have fundamental effects on the osteogenic program of adherent cells.
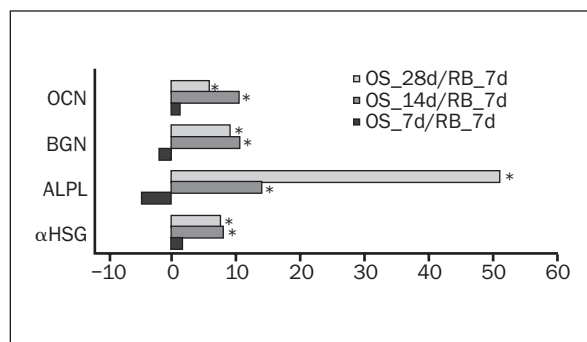
The differences observed between nanotopography and microtopography surfaces[20] suggest that specific regulatory information may be provided by the nanotopographic environments.

In this report, human MSC gene expression related to the process of osteoinduction is highlighted. The greatest differences between the microtopographic TiO surface and the superimposed nanotopography of the OS surface are noted for BMP2, BMP4, and BMP6 expression (Fig 6). The expression of these BMPs is central to the osteogenic program of the MSCs. Luu et al[31] showed that BMP2, BMP6, and BMP9 are particularly strong osteoinductive members of the BMP family. Here, BMP9 levels were not monitored. In another investigation using human MSCs, comparing BMP2, BMP4, BMP6, and BMP7, BMP6 is the most consistent and potent regulator of osteoblast differentiation and, of these BMPs, only BMP6 gene expression was detected prior to human MSC osteoblast differentiation. BMP6 induced the expression of type I collagen, osteocalcin, bone sialoprotein, and their regulatory transcription factors Cbfa1/Runx2 and Osterix.[32] BMP6 expression was most clearly distinguished and elevated in cells cultured on the OS surface. Whereas TGFβ1 expression has been measured as an index of osteogenesis in many studies using the osteoblast-like MG-63 cell line to evaluate surface topography effects, the changes observed for the TGFβ members of the superfamily were relatively modest (eg, Boyan et al[33]). This could reflect differences between the MG-63 osteosarcoma model and the human MSC model used here.

The temporal display of surface-specific changes is noteworthy. Early differences (day 7) were modest in comparison to some (eg, BMP6, biglycan) measured at 14 and 28 days. At 7 days, key inducers of osteogenesis such as RUNX2, SMAD1, and growth factors such as fibroblastic growth factor 2 and IGF2 were expressed at higher levels on OS surfaces compared to GB surfaces. The positive expression of these factors and their higher expression implicates the superimposed nanotopography in positive modulation of stem cell differentiation to osteoblasts. In a separate investigation, in vivo RUNX2 levels of implant adherent cells were also elevated on OS compared to GB surfaces.[34]

The display of differences in gene expression at later time points strongly suggests that greater osteogenesis occurred at the OS than on the GB surfaces. The culture layers displayed high levels of osteoinductive and osteogenic growth factors as well as higher levels of bone matrix proteins. It is not clear from this study which cellular mechanisms act to distinguish cell behavior at the nanotopography level from the microtopography level. However, other investigations suggest that the filipodial relationships with these surface features may be critical.[27] Further investigation using this model can focus on the earliest time points to identify immediate and early gene responses to elucidate mechanisms that promoted the changes observed here.

The differences observed at 28 days are physiologic alterations in the adherent multilayer culture system, suggesting that a similar endosseous implant can affect peri-implant accrual of bone mass. The significantly higher levels of osteoinductive and osteogenic factors observed in cell culture at 28 days suggest that the organization of forming tissues on nanotopographically enhanced implant surfaces in vivo may also experience more profound and sustained periods of surface-directed osteogenesis.

In conclusion, the human mesenchymal stem cell model provides valuable information concerning the influence of nanotopographic features of substrate topography on osteogenesis. Osteoinductive factors are expressed at higher levels in cells adherent to moderately rough surfaces embellished with nanotopographic features imparted by hydrofluoric acid treatment. These molecular studies are consistent with histologic and biomechanical assessments of titanium grit–blasted commercially pure titanium implants displaying a nanotopography following hydrofluoric acid treatment.

REFERENCES

1. Albrektsson T, Wennerberg A. Oral implant surfaces: Part 1—Review focusing on topographic and chemical properties of different surfaces and in vivo responses to them. Int J Prosthodont 2004;17:536–543.
2. Ivanoff CJ, Hallgren C, Widmark G, Sennerby L, Wennerberg A. Histologic evaluation of the bone integration of TiO(2) blasted and turned titanium microimplants in humans. Clin Oral Implants Res 2001;12:128–134.
3. Botticelli D, Berglundh T, Buser D, Lindhe J. The jumping distance revisited: An experimental study in the dog. Clin Oral Implants Res 2003;14:35–42.
4. Reyes CD, Petrie TA, Burns KL, Schwartz Z, Garcia AJ. Biomolecular surface coating to enhance orthopaedic tissue healing and integration. Biomaterials 2007;28:3228–3235.
5. Schliephake H, Aref A, Scharnweber D, Bierbaum S, Roessler S, Sewing A. Effect of immobilized bone morphogenic protein 2 coating of titanium implants on peri-implant bone formation. Clin Oral Implants Res 2005;16:563–569.
6. Liu H, Webster TJ. Nanomedicine for implants: A review of studies and necessary experimental tools. Biomaterials 2006;28:354–369.
7. Zinger O, Zhao G, Schwartz Z, et al. Differential regulation of osteoblasts by substrate microstructural features. Biomaterials 2005;26:1837–1847.
8. Park GE, Webster TJ. A review of nanotechnology for the development of better orthopedic implants. J Biomed Nanotechnol 2005;1:18–29.
9. Sato M, Webster TJ. Nanobiotechnology: Implications for the future of nanotechnology in orthopedic applications [review]. Expert Rev Med Devices 2004;1:105–114.
10. de Oliveira PT, Nanci A. Nanotexturing of titanium-based surfaces upregulates expression of bone sialoprotein and osteopontin by cultured osteogenic cells. Biomaterials 2004;25:403–413.
11. Schopper C, Moser D, Goriwoda W, et al. The effect of three different calcium phosphate implant coatings on bone deposition and coating resorption: A long-term histological study in sheep. Clin Oral Implants Res 2005;16:357–368.
12. Okada M, Furuzono T. Nano-sized ceramic particles of hydroxyapatite calcined with an anti-sintering agent. J Nanosci Nanotechnol 2007;7:848–851.
13. Kobayashi T, Itoh S, Nakamura S, Nakamura M, Shinomiya K, Yamashita K. Enhanced bone bonding of hydroxyapatite-coated titanium implants by electrical polarization. J Biomed Mater Res A 2007;82:145–151.
14. Sato M, Aslani A, Sambito MA, Kalkhoran NM, Slamovich EB, Webster TJ. Nanocrystalline hydroxyapatite/titania coatings on titanium improves osteoblast adhesion. J Biomed Mater Res A 2008;84:265–272.
15. Orsini G, Piattelli M, Scarano A, et al. Randomized, controlled histologic and histomorphometric evaluation of implants with nanometer-scale calcium phosphate added to the dual acid-etched surface in the human posterior maxilla. J Periodontol 2007;78:209–218.
16. Sul YT, Byon ES, Jeong Y. Biomechanical measurements of calcium-incorporated oxidized implants in rabbit bone: Effect of calcium surface chemistry of a novel implant. Clin Implant Dent Relat Res 2004;6:101–110.
17. Sul YT, Johansson C, Wennerberg A, Cho LR, Chang BS, Albrektsson T. Optimum surface properties of oxidized implants for reinforcement of osseointegration: Surface chemistry, oxide thickness, porosity, roughness, and crystal structure. Int J Oral Maxillofac Implants. 2005;20:349–359.

18. Berglundh T, Abrahamsson I, Albouy JP, Lindhe J. Bone healing at implants with a fluoride-modified surface: An experimental study in dogs. Clin Oral Implants Res 2007;18:147–152.

19. Cooper LF, Zhou Y, Takebe J, et al. Fluoride modification effects on osteoblast behavior and bone formation at TiO$_2$ grit-blasted c.p. titanium endosseous implants. Biomaterials 2006;27:926–936.

20. Masaki C, Schneider GB, Zaharias R, Seabold D, Stanford C. Effects of implant surface microtopography on osteoblast gene expression. Clin Oral Implants Res 2005;16:650–656.

21. Pesskova V, Kubies D, Hulejova H, Himmlova L. The influence of implant surface properties on cell adhesion and proliferation. J Mater Sci Mater Med 2007;18:465–473.

22. Gretzer C, Emanuelsson L, Liljensten E, Thomsen P. The inflammatory cell influx and cytokines changes during transition from acute inflammation to fibrous repair around implanted materials. J Biomater Sci Polym Ed 2006;17:669–687.

23. Buser D, Broggini N, Wieland M, et al. Enhanced bone apposition to a chemically modified SLA titanium surface. J Dent Res 2004;83:529–533.

24. Jaiswal N, Haynesworth SE, Caplan AI, Bruder SP. Osteogenic differentiation of purified, culture-expanded human mesenchymal stem cells in vitro. J Cell Biochem 1997;64:295–312.

25. Stout KJ, Sullivan PJ, Dong WP, et al. The Development of Methods for Characterisation of Roughness in Three Dimensions. University of Birmingham: EUR 15178 EN of Commission of the European Communities, 1993.

26. Wang K, Yamamoto H, Chin JR, Werb Z, Vu TH. Epidermal growth factor receptor-deficient mice have delayed primary endochondral ossification because of defective osteoclast recruitment. J Biol Chem 2004;279:53484–53456.

27. Nanes MS. Tumor necrosis factor-alpha: Molecular and cellular mechanisms in skeletal pathology [review]. Gene 2003;321:1–15.

28. Dalby MJ, McCloy D, Robertson M, Wilkinson CD, Oreffo RO. Osteoprogenitor response to defined topographies with nanoscale depths. Biomaterials 2006;27:1306–1315.

29. Oliveira PT, Zalzal SF, Beloti MM, Rosa AL, Nanci A. Enhancement of in vitro osteogenesis on titanium by chemically produced nanotopography. J Biomed Mater Res A 2007;80:554–564.

30. Isa ZM, Schneider GB, Zaharias R, Seabold D, Stanford CM. Effects of fluoride-modified titanium surfaces on osteoblast proliferation and gene expression. Int J Oral Maxillofac Implants 2006;21:203–211.

31. Luu HH, Song WX, Luo X, et al. Distinct roles of bone morphogenetic proteins in osteogenic differentiation of mesenchymal stem cells. J Orthop Res 2007;25:665–677.

32. Friedman MS, Long MW, Hankenson KD. Osteogenic differentiation of human mesenchymal stem cells is regulated by bone morphogenetic protein-6. J Cell Biochem 2006;98:538–554.

33. Boyan BD, Batzer R, Kieswetter K, et al. Titanium surface roughness alters responsiveness of MG63 osteoblast-like cells to 1 alpha,25-(OH)2D3. J Biomed Mater Res 1998;39:77–85.

34. Guo J, Padilla RJ, Ambrose W, De Kok IJ, Cooper LF. The effect of hydrofluoric acid treatment of TiO$_2$ grit blasted titanium implants on adherent osteoblast gene expression in vitro and in vivo. Biomaterials 2007;28:5418–5425.